International Journal of Mathematics and Physical Sciences Research ISSN 2348-5736 (Online)
Vol. 11, Issue 1, pp: (101-121), Month: April 2023 - September 2023, Available at: www.researchpublish.com

A MODEL ON MHD CONVECTIVE TIN-OXIDE (TiO_2) NANOFLUID FLOW OVER A CYLINDERICAL POROUS PLATE

Tombotamunoa W. J. Lawson [1*], Isobeye George [1], Alalibo T. Ngiangia,[2]

[1]Department of Mathematics/Statistics, Ignatius Ajuru University of Education, PMB 5047, Port Harcourt, Nigeria.
[2]Department of Physics, University of Port Harcourt, PMB 5323 Choba, Port Harcourt, Nigeria.

[*]Corresponding Author: Tombotamunoa W. J. Lawson

DOI: https://doi.org/10.5281/zenodo.8362486

Published Date: 20-September-2023

Abstract: **In this study, a model of MHD convective tin-oxide(TiO_2) nanofluid flow over a cylindrical porous plate was examined. The governing equations of continuity, momentum, energy, and concentration modelled in terms of partial differential equations with boundary conditions were non-dimensionalised using the Buckingham's π-theorem and then were transformed into ordinary differential equations using the regular perturbation technique, each of these equations was solved in isolation using Frobenius Method which gave the analytic solutions. The solutions obtained for the momentum, energy, and concentration were subjected to analysis which gave the results for the temperature profile, concentration profile, and velocity profile graphically. It was observed that, when the radiation parameter was increased, the temperature profile dropped; as the chemical reaction was increased, the concentration profile and the velocity profile were reduced; again as the magnetic field number was increased, it lowered the profile of the velocity. The velocity profile was enhanced with an increase in the porosity parameter, and this, as a result, tended to increase in the size of the pore spaces of the porous medium; the concentration profile, temperature profile, and velocity profile all improved as the nanofluid volume fraction increased.**

Keywords: **Nanofluid, MHD flow, Convection, Cylindrical Porous Plate, Analytical Solutions.**

1. INTRODUCTION

Nanofluids are created by suspending nanoparticles (particles with a "size" of less than 1μm) in liquids known as base fluids, which have average diameters of less than 100 nm in standard heat transfer fluids including water, ethylene glycol, and oil. When disseminated uniformly and suspended stably in host fluids, a modest number of guest nanoparticles can significantly improve the thermal characteristics of the host fluids. Choi (1995) used the term nanofluids (nanoparticle fluid suspensions) to designate a novel class of nanotechnology-based heat transfer fluids with thermal qualities superior to their host fluids or conventional fluids. Nanofluid technology as a novel inter-disciplinary subject where nanotechnology, nanoscience, and thermal engineering interface, has mostly developed during the last decade (Li, 1998; Feng et al., 2006; Kulkarni et al., 2008; Khan et al., 2020; Mukherjee & Paria, 2013; Maleki et al., 2019). According to Xuan and Li (2003), a wide range of engineering applications, such as automotive and air conditioning cooling, solar and power plant cooling, transformer oil cooling, improving diesel generator efficiency, nuclear reactors, and defense and space, are the main driving forces for nanofluids research. Jang and Choi (2004) designed a new cooler that combined a microchannel heat sink with nanofluids. When compared to a device that used pure water as the working medium, the cooling performance was improved. A nanofluid as a coolant in a microchannel heat exchanger to cool crystal silicon mirrors used in high-intensity X-ray sources, and found that the nanofluid significantly improved cooling rates over conventional water-cooled and liquid-nitrogen-cooled microchannel heat exchangers (Lee et al., 1999). The flow and heat transfer characteristics of a water-based nanofluid inside a grooved channel with a rotating heat source are quantitatively explored in this work for the influence of

an oriented magnetic field on mixed convection flow (Mokaddes et al., 2019). According to several research initiatives from the late 1990s and the first decade of the twenty-first century, adding relatively modest concentrations of nanoparticles to frequently used base fluids like water and ethyl glycol boosted the effective thermal conductivity of these mixes dramatically (Choi, 1995; Touloukia et al., 1970; Yu et al., 2010; Hwarig et al., 2007; Zhu et al., 2007; Li et al., 2007; Hussian et al., 2018; Chamkha, 2011; Adenyan, 2015; Rawar et al., 2016). Brownian motion's impact in increasing the thermal conductivity of nanofluids was investigated by Gupta and Kumar (2007). Cheng et al. (2007) investigated ethylene glycol-based nanofluids with TiO_2 nanoparticles at a concentration of 0.5 percent to 8.0 percent by weight at 20°–60°C using both experimental and theoretical methods. Under those conditions, they found Newtonian behavior, with shear viscosity being a strong function of temperature and nanoparticle loading. Das et al. (2003) on the other hand, conducted a similar work with water-Al_2O_3 nanofluids, but only reported on shear thinning behavior. Maiga et al. (2006) investigated the forced convection of alumina particles suspended in ethylene glycol and water in a uniformly heated tube. They discovered that the heat transfer coefficient and wall shear stress rose as the nanoparticle volume percent and Reynolds number increased. Nanofluids are thought to provide a number of benefits over traditional heat transfer fluids. Their thermophysical properties, on the other hand, are unknown at this early point in their development. As a result, it's impossible to estimate their full potential. This is demonstrated by looking at their thermohydraulic performance in a tube with a uniform wall heat flux for both laminar and turbulent fully developed forced convection. Two different literature models were used to express these properties in terms of particle loading, and they produce very different qualitative and quantitative results in two types of problems: replacing a simple fluid with a nanofluid in a given installation and designing an elementary heat transfer installation for a simple fluid or a nanofluid (Mansour et al., 2007). Convection is the heat transfer that occurs between a flowing fluid and a surface when their temperatures are different. Many have hailed nanofluids as the heat transfer medium of the future. Heat is transmitted through convection, a combination of conduction and fluid advection, in all practical energy systems containing fluids. As a result, rather than conduction, the phenomenon of nanofluid convection would be of technological interest. Sheikholeslami et al. (2015) examined the thermal radiation on MHD nanofluid, by using similarity transformation for temperature, concentration, and velocity the basic equations governing the mass transfer, heat transfer and flow were coverted to a system of ordinary differential equations, and these equations were subjected boundary conditions which were numerically solved by using the technique of Runge-Kutta Fourth- order. MHD is the acronym for magnetohydrodynamics which is defined as the study of how magnetic fields interact with moving, electrically conducting fluids (Schnack, 2009). Nanofluids, which are made up of a mixture of base fluids and nanoparticles, must be electrically conducting and hence vulnerable to magnetic fields. Many industrial and engineering applications rely on the flow of electrically conducting fluids in the presence of a magnetic field. The impact of a uniform magnetic field on nanofluid flow between two circular cylinders was explored (Sheikholeslami et al., 2018). Hayat et al. (2015) investigated the “MHD three-dimensional flow of nanofluid with velocity slip and nonlinear thermal radiation”, alumina was treated as a nanoparticle and water as a base fluidand , the nonlinear system for temperature distribution was analyzed and solved. Zeeshan et al. (2012), studied the MHD flow of third-grade nanofluid between coaxial porous cylinders. An analytical analysis was performed to investigate the effect of a chemical reaction on the MHD flow of a nanofluid in an expanding or contracting porous pipe in the presence of a heat source/sink (Srinivas et al., 2016). The magnetic field may be used to control heat transfer and fluid flow, and it can also be used to maximize thermodynamic efficiency in a variety of fields. Heat transfer increases using nanofluids and porous inserts are two common methods (Aminian et al., 2020). For both constant and variable viscosity, two types of series solutions were presented. In this work, a model of MHD convective tin-oxide (TiO_2) nanofluid flow over a cylindrical porous plate is investigated.

2. MODELING THE PHYSICAL PROBLEM

An unsteady, oscillatory, incompressible, radiating tin-oxide nanofluid flow with two infinite concentric surfaces of inner and outer radii r^l and r respectively, with a free stream frequency for the inner and outer parts of the cylinder with v representing the velocity of the nanofluid is considered. The outer cylinder is at rest as the inner cylinder is moving upward and downward. The effect of the induced magnetic field is neglected on the assumption that it is minimal. Using Boussinesq’s approximation, the governing hydrodynamic partial differential equations in the cylindrical form of the nanofluid flow are given as

$$\frac{\partial \rho_{nf}}{\partial t^{'}} + \frac{1}{r^{'}}\frac{\partial}{\partial r}\left(\rho_{nf} r^{'} v_r\right) = 0 \qquad (1)$$

$$\rho_{nf}\left(\frac{\partial v_r}{\partial t^t}+v_r\frac{\partial v_r}{\partial r^t}\right)=\mu_{nf}\left[\frac{\partial}{\partial r^t}\left(\frac{1}{r^t}\frac{\partial}{\partial r^t}\left(r^t v_r\right)\right)\right]+g\rho_{nf}\beta_{nf}(T^t-T_\infty)+g\rho_{nf}\beta^t{}_{nf}(C^t-C_\infty)$$
$$-\frac{\mu_{nf}}{k^t}v_r-\sigma\beta_0^2 v_r=0 \quad (2)$$

$$(\rho C_p)_{nf}\left(\frac{\partial T}{\partial t^t}+v_r\frac{\partial T}{\partial r^t}\right)=K_{nf}\left[\frac{1}{r^t}\frac{\partial}{\partial r^t}r^t\left(\frac{\partial T}{\partial r^t}\right)\right]-\frac{\partial q}{\partial r} \quad (3)$$

$$(\rho C_p)_{nf}\left(\frac{\partial C^t}{\partial t^t}+v_r\frac{\partial C^t}{\partial r^t}\right)=D_{nf}\left[\frac{1}{r^t}\frac{\partial}{\partial r^t}r^t\left(\frac{\partial C^t}{\partial r^t}\right)\right]-K_r^2C^t \quad (4)$$

with the boundary conditions, $v_r(0,t)=0$, $v_r(1,t)=1$, $T(0,t)=0$, $T(1,t)=1$, $C^t(0,t)=0$, $C^t(1,t)=1$ (Ngiangia and Akaezue 2019).

where $v_r\ (r,t)$ denotes the nanofluid velocity, $T\ (r,t)$ is the temperature of the nanofluid, $C^t\ (r,t)$ is the concentration of the nanofluid, t is the time, r^t is the radius of the nanoparticles, ρ_{nf} is the density of nanofluids, μ_{nf} is the nanofluid dynamic viscosity coefficient, σ is the conductivity of the base fluid, g is the acceleration due to gravity, B_0^2 is the magnetic field, k_r^2 is the chemical reaction term, k^t is the permeability or porosity parameter, $\rho_{nf}\beta_{nf}$ is the thermal expansion coefficient of the nanofluids due to temperature, g is the acceleration due to gravity, $(\rho C_p)_{nf}$ is the heat capacitance of the nanofluids, $\rho_{nf}\beta^t{}_{nf}$ is thermal expansion coefficient of the nanofluids due to Concentration, K_{nf} is the thermal conductivity of the nanofluid, D_{nf} is the Chemical molecular diffusivity the nanofluid, q is the radiative heat flux.

In this research work, the Hamilton and Crosser (1962) models for thermal conductivity and dynamic viscosity are used, being valid for both spherical and non-spherical shape nanoparticles. $\mu_{nf}=\mu_f(1+a\phi+b\phi^2)$ (5)

$$\frac{k_{nf}}{k_f}=\frac{k_s+(n-1)k_f+(n-1)(k_s-k_f)\phi}{k_s+(n-1)k_f-(k_s-k_f)\phi} \quad (6)$$

According to Loganathan et al. (2013) and Asma et al. (2015),

$$\left.\begin{aligned}\rho_{nf}&=(1-\phi)\rho_f+\phi\rho_s\\(\rho\beta)_{nf}&=(1-\phi)(\rho\beta)_f+\phi(\rho\beta)_s\\(\rho C_\rho)_{nf}&=(1-\phi)(\rho C_p)_f+\phi(\rho C_p)_s\end{aligned}\right\} \quad (7)$$

where ϕ is the nanoparticles volume fraction, ρ_f and ρ_s are the densities of the base fluids and solids particles, β_f and β_s are the thermal expansion due to temperature of base fluids and solids nanoparticles, K_f and K_S are the thermal conductivity of the fluid and solids nanoparticles, $(c_p)_f$ and $(c_p)_s$ are the specific heat capacities of solid nanoparticles and base fluids at constant pressure, μ_f is the dynamic viscosity coefficient of the fluid, a and b are constants and depend on the particle shapes as given in Table 1.

The n appearing in Equation (6) is the empirical shape factor given by n = 3/Ψ, where Ψ is the sphericity defined as the ratio between the surface area of the sphere and the surface area of the real particle with equal volumes. The values of Ψ for different shape particles are given in Table 2.

In addition to the above, some physical properties of the base fluid and nanoparticles are given in Table 3.

In the work of Makinde and Mhone (2005), the temperature of the plates T_0 , T_w are assumed high enough to produce radiative heat transfer. According to Cogley et al. (1968), for an optically thin medium with relatively low density, the radiative heat flux is given by

$$\frac{\partial q}{\partial y} = 4\delta^2 (T - T_0) \tag{8}$$

where δ is the radiation absorption coefficient.

Table 1: Constant *a* and *b* empirical shape factors, (Timofeeva et al., 2009 and Aaiza et al., 2015).

Model	Platelet	Blade	Cylinder	Brick
a	37.1	14.6	13.5	1.9
b	612.6	123.3	904.4	471.4

Table 2: Shericity Ψ for the different nanoparticles shapes, (Timofeeva et al., 2009 and Aaiza et al., 2015).

Model	Platelet	Blade	Cylinder	Brick
Ψ	0.52	0.36	0.62	0.81

Applying the following dimensionless variables using Buckingham's π- theorem

$$r = \frac{r'}{d} \qquad v = \frac{v_r}{v_0} \qquad t = \frac{t' v_0}{d} \qquad \frac{1}{k} = \frac{d^2 \rho_f}{k' \rho_{nf}}$$

$$\theta = \frac{T' - T_\infty}{T_w - T_\infty} \qquad C = \frac{C' - C_\infty}{C_w - C_\infty} \qquad k_\infty = \frac{k_r^2 T_\infty}{v_0^2} \qquad N = \frac{4\sigma^2 d^2}{k_f}$$

$$M = \frac{\sigma B_0^2 \mu_{nf} \rho_f}{\mu_f \rho_{nf} v_r} \qquad \mathrm{Re}^{-1} = \frac{\mu_{nf} \rho_f}{\mu_f \rho_{nf}} \qquad Sc^{-1} = \frac{D}{\nu} \qquad \mathrm{Pr} = \frac{\nu \rho C_p}{(\rho C_p)_{nf} k_f}$$

$$Gr_\theta = \frac{g \beta_{nf} (T' - T_\infty) \mu_{nf}}{U_0 v_r^2 \beta_f} \qquad Gr_C = \frac{g \beta'_{nf} (C' - C_\infty) \mu_{nf}}{U_0 v_r^2 \beta'_f}$$

Applying dimensionless variables above in equations (1), (2), (3) and (4), the modelled equations are transformed into

$$\frac{\partial}{\partial t}\left(\frac{\rho_{nf}}{\rho_f}\right) + \frac{1}{r}\frac{\partial}{\partial r}\left(\frac{\rho_{nf} r v}{\rho_f}\right) = 0 \tag{9}$$

$$\frac{\partial v}{\partial t} + v\frac{\partial v}{\partial r} = \mathrm{Re}^{-1} L_1 \left(\frac{\partial^2 v}{\partial r^2} + \frac{1}{r}\frac{\partial v}{\partial r} - \frac{v}{r^2}\right) + Gr_\theta \theta L_2 + Gr_C C L_3 - \left(\frac{L_6}{k} + M\right) v = 0 \tag{10}$$

$$\frac{\partial \theta}{\partial t}+v\frac{\partial \theta}{\partial r}=\mathrm{Pr}^{-1}L_5\left(\frac{\partial^2\theta}{\partial r^2}+\frac{1}{r}\frac{\partial \theta}{\partial r}\right)-NL_4\theta \tag{11}$$

$$\frac{\partial C}{\partial t}+v\frac{\partial C}{\partial r}=Sc^{-1}L_4\left(\frac{\partial^2 C}{\partial r^2}+\frac{1}{r}\frac{\partial C}{\partial r}\right)-k_\infty L_4 C \tag{12}$$

Subject to the boundary conditions

$$v(0,t)=0,\quad v(1,t)=e^{\omega t}\quad t>0 \tag{13}$$

$$\theta(0,t)=0,\quad \theta(1,t)=e^{\omega t}\quad t>0 \tag{14}$$

$$C(0,t)=0,\quad C(1,t)=e^{\omega t}\quad t>0 \tag{15}$$

Where r is the dimensionless coordinate, k_∞ is the dimensionless chemical reaction term, N is the dimensionless radiation parameter, d is the diameter, k is the dimensionless porosity parameter, M is the magnetic parameter also called the Hartmann number, Re is called the Reynold number, Sc is the Schmidt number, Pr is the Prandtl number, Gr_T is the thermal Grashof number, Gr_C is the modified Grashof number.

Further, we define:

$$L_1=\frac{1+a\phi+b\phi^2}{1-\phi-\phi\frac{\rho_s}{\rho_f}} \qquad L_2=1-\phi-\phi\frac{\beta_s}{\beta_f} \qquad L_3=1-\phi-\phi\frac{\beta'_s}{\beta'_f}$$

$$L_4=\left[1-\phi-\phi\frac{(\rho C_p)_s}{(\rho C_p)_f}\right]^{-1} \qquad L_5=\frac{k_s+(n-1)k_f+(n-1)(k_s-k_f)\phi}{k_s+(n-1)k_f-(k_s-k_f)\phi}L_4 \qquad L_6=1+a\phi+b\phi^2$$

$$J_1=\mathrm{Re}^{-1}L_1 \qquad J_2=Gr_\theta L_2 \qquad J_3=Gr_C L_3 \qquad J_4=\frac{L_6}{k}+M$$

$$w_1=\mathrm{Pr}^{-1}L_5 \qquad w_2=\mathrm{N}L_4 \qquad E_1=Sc^{-1}L_4 \qquad E_2=k_\infty L_4$$

Table 3 Thermophysical properties of water and tinoxide nanoparticles, (Loganathan et al. (2013) and Asma et al. (2015)).

Model	$\rho(kgm^{-3})$	$C\rho(kg^{-1}k^{-1})$	$k(Wm^{-1}k^{-1})$	$\beta\times10^{-5}(k^{-1})$
H_2O	997.1	4179	0.613	21
TiO_2	4250	686.2	8.9528	0.9

Method of Solution

Assuming the nanofluid under consideration is incompressible, as a necessary condition for engineering and science applications. The solution of equation (9) yields

$$\frac{1}{r}\frac{\partial}{\partial t}\left(\frac{\rho_{nf}rv}{\rho_f}\right)=0$$

$$v=\frac{Q}{r} \tag{16}$$

where Q is an integration constant.

Using the transformation technique used by Ngiangia and Orukari (2021), a regular perturbation of the form

$$v(r,t) = v_0(r) + v_1(r)e^{-\omega t} \quad (17)$$

$$\theta(r,t) = \theta_0(r) + \theta_1(r)e^{-\omega t} \quad (18)$$

$$C(r,t) = C_0(r) + C_1(r)e^{-\omega t} \quad (19)$$

is selected

where ω is a free stream angular velocity.

Putting equation (16) into equations (10) - (12) and applying the regular perturbation technique by substituting equations (17), - (19) into the simplified equations gives:

$$J_1\frac{d^2v_0}{dr^2}+\left(\frac{J_1-\mathrm{Q}}{r}\right)\frac{dv_0}{dr}-\left(\frac{J_1}{r^2}+J_4\right)v_0+J_2\theta_0+J_3C_0=0 \quad (20)$$

$$J_1\frac{d^2v_1}{dr^2}+\left(\frac{J_1-\mathrm{Q}}{r}\right)\frac{dv_1}{dr}-\left(\frac{J_1}{r^2}+J_4-\omega\right)v_1+J_2\theta_1+J_3C_1=0 \quad (21)$$

$$w_1\frac{d^2\theta_0}{dr^2}+\left(\frac{w_1-\mathrm{Q}}{r}\right)\frac{d\theta_0}{dr}-w_2\theta_0=0 \quad (22)$$

$$w_1\frac{d^2\theta_1}{dr^2}+\left(\frac{w_1-\mathrm{Q}}{r}\right)\frac{d\theta_1}{dr}+(\omega-w_2)\theta_1=0 \quad (23)$$

$$E_1\frac{d^2C_0}{dr^2}+\left(\frac{E_1-\mathrm{Q}}{r}\right)\frac{dC_0}{dr}-E_2C_0=0 \quad (24)$$

$$E_1\frac{d^2C_1}{dr^2}+\left(\frac{E_1-\mathrm{Q}}{r}\right)\frac{dC_1}{dr}+(\omega-E_2)C_1=0 \quad (25)$$

Subject to the associated boundary conditions

$$v_0(0,t)=0,\ v_0(1,t)=e^{\omega t},\ v_1(0,t)=0,\ v_1(1,t)=e^{\omega t},\ \theta_0(0,t)=0,\ \theta_0(1,t)=e^{\omega t},$$

$$\theta_1(0,t)=0,\theta_1(1,t)=e^{\omega t},\ C_0(0,t)=0,\ C_0(1,t)=e^{\omega t},\ C_1(0,t)=0,\ \ C_1(1,t)=e^{\omega t}$$

With the presence of a singular point, equation (20) – (25) is tested and shown finite, implying that it is analytic (Dass and Rama, 2000, Gupta, 2005, and Raisinghania, 2011), and so an analytic feasible solution is attainable. A solution of this kind can be found using the Frobenius approach.

$$\theta_0(r)=\sum_{k=0}^{\infty}a_k r^{(m+k)} \quad (26)$$

is assumed.

Substituting equations (26) into equations (22) after simplification, the expression obtained an indicial equation of the form

$$m\left[w_1(m-1)+w_1-\mathrm{Q}\right]a_0=0 \qquad (a_0\neq 0) \quad (27)$$

the solution is obtained as

$$m = 0, \text{ or } m = \frac{\mathrm{Q}}{w_1} \tag{28}$$

the recurrence relation is

$$a_{k+2} = \frac{w_2}{(m+k+2)\left[w_1(m+k+1)+w_1-\mathrm{Q}\right]}a_k \tag{29}$$

and the solution after imposing the boundary conditions is given by

$$\theta_0(r) = \frac{e^{wt}}{\left(1+\frac{w_2}{2\mathrm{Q}+4w_1}+\ldots\right)}\left(r^{\frac{Q}{w_1}} + \frac{w_2 r^{2+\frac{\mathrm{Q}}{w_1}}}{2\mathrm{Q}+4w_1}+\ldots\right) \tag{30}$$

The recurrence relation of equation (23) using the same approach is given as

$$a_{k+2} = \frac{(\omega - w_2)}{(m+k+2)\left[w_1(m+k+1)+w_1-\mathrm{Q}\right]}a_k \tag{31}$$

and solution after imposing the boundary conditions yield to

$$\theta_1(r) = \frac{e^{wt}}{\left(1+\frac{(\omega-w_2)}{2Q+4w_1}+\ldots\right)}\left(r^{\frac{Q}{w_1}} + \frac{(\omega-w_2)r^{2+\frac{Q}{w_1}}}{2Q+4w_1}+\ldots\right) \tag{32}$$

Substituting equations (26) into equations (24) after simplification, the expression obtained an indicial equation of the form

$$m\left[E_1(m-1)+E_1-Q\right]a_0 = 0 \qquad (a_0 \neq 0) \tag{33}$$

the solution is obtained as

$$m = 0, \qquad m = \frac{Q}{E_1}$$

The recurrence relation of equation (24) using the same approach is given as

$$a_{k+2} = \frac{E_2}{(m+k+2)\left[E_1(m+k+1)+E_1-Q\right]}a_k \tag{34}$$

and solution after imposing the boundary conditions yield to

$$C_0(r) = \frac{e^{wt}}{\left(1+\frac{E_2}{2Q+4E_1}+\ldots\right)}\left(r^{\frac{Q}{E_1}} + \frac{w_2 r^{2+\frac{Q}{E_1}}}{2Q+4E_1}+\ldots\right) \tag{35}$$

Using the same approach, then the recurrence relation is found to be:

$$a_{k+2} = \frac{(\omega - E_2)}{(m+k+2)\left[E_1(m+k+1)+E_1-Q\right]}a_k \tag{36}$$

and solution after imposing the boundary conditions yield to

$$C_1 = \frac{e^{wt}}{\left(1+\frac{(\omega-E_2)}{2Q+4E_1}+\ldots\right)}\left(r^{\frac{Q}{E_1}}+\frac{(\omega-E_2)r^{2+\frac{Q}{E_1}}}{2Q+4E_1}+\ldots\right) \tag{37}$$

Rewriting equation (20) yields

$$J_1\frac{d^2V_0}{dr^2}+r^{-1}(J_1-Q)\frac{dV_0}{dr}-r^{-2}J_1V_0+J_4V_0=-J_2r^a\left(A_{11}+A_{12}r^2\right)-J_3r^b\left(B_{11}+B_{12}r^2\right) \tag{38}$$

where

$$a=\frac{Q}{w_1}, \qquad A_{11}=\frac{e^{\omega t}(2Q+4w_1)}{2Q+4w_1+w_2} \qquad A_{12}=\frac{w_2e^{\omega t}}{2Q+4w_1+w_2}$$

$$b=\frac{Q}{E_1}, \qquad B_{11}=\frac{e^{\omega t}(2Q+4E_1)}{2Q+4E_1+E_2} \qquad B_{12}=\frac{E_2e^{\omega t}}{2Q+4E_1+E_2}$$

The solution of the complimentary part in equation (38) yields

$$v_c = A_5r^{\frac{Q+\sqrt{Q^2+4J_1^2}}{2J_1}}\left(1+\frac{J_4r^2}{\left(\frac{Q+\sqrt{Q^2+4J_1^2}}{2J_1}+2\right)\left(J_1\left[\frac{Q+\sqrt{Q^2+4J_1^2}}{2J_1}\right]+2J_1-Q\right)-J_1}+\ldots\right)$$
$$+B_5r^{\frac{Q-\sqrt{Q^2+4J_1^2}}{2J_1}}\left(1+\frac{J_4r^2}{\left(\frac{Q-\sqrt{Q^2+4J_1^2}}{2J_1}+2\right)\left(J_1\left[\frac{Q-\sqrt{Q^2+4J_1^2}}{2J_1}\right]+2J_1-Q\right)-J_1}+\ldots\right) \tag{39}$$

$$v_p = a_{11}r^a+a_{12}r^{2+a}+a_{13}r^{1+a}+a_{14}r^a+b_{11}r^b+b_{12}r^{2+b}+b_{13}r^{1+b}+b_{14}r^b \tag{40}$$

The solution of the particular integral in equation (38) yields

$$v_P=\frac{J_2A_{12}}{J_4}r^{2+a}+\frac{J_3B_{12}}{J_4}r^{2+b} \tag{41}$$

The complete solution, which is a combination of the complimentary function and the particular integral after the imposition of the boundary conditions then take the form:

$$V_0 = A_5 r^{\frac{Q+\sqrt{Q^2+4J_1^2}}{2J_1}}\left(1+\frac{J_4 r^2}{\left(\frac{Q+\sqrt{Q^2+4J_1^2}}{2J_1}+2\right)\left(J_1\left[\frac{Q+\sqrt{Q^2+4J_1^2}}{2J_1}\right]+2J_1-Q\right)-J_1}+\ldots\right)$$

$$+B_5 r^{\frac{Q-\sqrt{C^2+4J_1^2}}{2J_1}}\left(1+\frac{J_4 r^2}{\left(\frac{Q-\sqrt{Q^2+4J_1^2}}{2J_1}+2\right)\left(J_1\left[\frac{Q-\sqrt{Q^2+4J_1^2}}{2J_1}\right]+2J_1-Q\right)-J_1}+\ldots\right) \quad (42)$$

$$+\frac{J_2 A_{12}}{J_4}r^{2+a}+\frac{J_3 B_{12}}{J_4}r^{2+b}$$

Similarly, adopting the same approach and procedure:

$$V_1 = A_6 r^{\frac{Q+\sqrt{Q^2+4J_1^2}}{2J_1}}\left(1+\frac{(\omega-J_4)r^2}{\left(\frac{Q+\sqrt{Q^2+4J_1^2}}{2J_1}+2\right)\left(J_1\left[\frac{Q+\sqrt{Q^2+4J_1^2}}{2J_1}\right]+2J_1-Q\right)-J_1}+\ldots\right)$$

$$+B_6 r^{\frac{Q-\sqrt{Q^2+4J_1^2}}{2J_1}}\left(1+\frac{(\omega-J_4)r^2}{\left(\frac{Q-\sqrt{Q^2+4J_1^2}}{2J_1}+2\right)\left(J_1\left[\frac{Q-\sqrt{Q^2+4J_1^2}}{2J_1}\right]+2J_1-Q\right)-J_1}+\ldots\right) \quad (43)$$

$$+\frac{J_2 R_{12}}{(\omega-J_4)}r^{2+a}+\frac{J_3 S_{12}}{(\omega-J_4)}r^{2+b}$$

Using the Taylor series expansion of $r^{\frac{Q+\sqrt{Q^2+4J_1^2}}{2J_1}}$ in equation (42) and equation (43), about the point $r = 1$and ignoring powers of $r > 1$, with the simplification of equation (42) and equation (43), after imposing the boundary conditions, also substituting equations (30), (32), (35), (37), (42) and (43) into equations (17), (18) and (19) respectively after simplification takes the form

$$\theta(r,t)=\frac{e^{\omega t}(2Q+4w_1)}{2Q+4w_1+w_2}r^{\frac{Q}{w_1}}+\frac{w_2}{2Q+4w_1+w_2}r^{2+\frac{Q}{w_1}}+\frac{(2Q+4w_1)}{2Q+4w_1+w_2}r^{\frac{Q}{w_1}}+\frac{(\omega-w_2)}{2Q+4w_1+w_2}r^{2+\frac{Q}{w_1}} \quad (44)$$

$$C(r,t)=\frac{e^{\omega t}(2Q+4E_1)}{2Q+4E_1+E_2}r^{\frac{C}{E_1}}+\frac{E_2}{2Q+4E_1+E_2}r^{2+\frac{Q}{E_1}}+\frac{(2Q+4E_1)}{2Q+4E_1+E_2}r^{\frac{Q}{E_1}}+\frac{(\omega-w_2)}{2Q+4E_1+E_2}r^{2+\frac{Q}{E_1}} \quad (45)$$

$$v(r,t) = A_5 r^{\frac{Q+\sqrt{Q^2+4J_1^2}}{2J_1}}\left(1+\frac{J_4 r^2}{\left(\frac{Q+\sqrt{Q^2+4J_1^2}}{2J_1}+2\right)\left(J_1\left[\frac{Q+\sqrt{Q^2+4J_1^2}}{2J_1}\right]+2J_1-Q\right)-J_1}+\ldots\right)$$

$$+B_5 r^{\frac{Q-\sqrt{Q^2+4J_1^2}}{2J_1}}\left(1+\frac{J_4 r^2}{\left(\frac{Q-\sqrt{Q^2+4J_1^2}}{2J_1}+2\right)\left(J_1\left[\frac{Q-\sqrt{Q^2+4J_1^2}}{2J_1}\right]+2J_1-Q\right)-J_1}+\ldots\right)$$

$$+\frac{J_2 A_{12}}{J_4}r^{2+a}+\frac{J_3 B_{12}}{J_4}r^{2+b}$$

$$+e^{-\omega t}\left(\begin{array}{l} A_6 r^{\frac{Q+\sqrt{Q^2+4J_1^2}}{2J_1}}\left(1+\frac{(\omega-J_4)r^2}{\left(\frac{Q+\sqrt{Q^2+4J_1^2}}{2J_1}+2\right)\left(J_1\left[\frac{Q+\sqrt{Q^2+4J_1^2}}{2J_1}\right]+2J_1-Q\right)-J_1}+\ldots\right) \\ +B_6 r^{\frac{Q-\sqrt{Q^2+4J_1^2}}{2J_1}}\left(1+\frac{(\omega-J_4)r^2}{\left(\frac{Q-\sqrt{Q^2+4J_1^2}}{2J_1}+2\right)\left(J_1\left[\frac{Q-\sqrt{Q^2+4J_1^2}}{2J_1}\right]+2J_1-Q\right)-J_1}+\ldots\right) \\ +\frac{J_2 R_{12}}{(\omega-J_4)}r^{2+a}+\frac{J_3 S_{12}}{(\omega-J_4)}r^{2+b} \end{array}\right) \quad (46)$$

3. RESULTS AND DISCUSSION

Results

To get numerical validation and physical insight into the problem, the parameters values used (Aaiza et al., 2015) are

Re = 1000, 1500, 2000, 2500, 3000; M = 1, 2, 3, 4, 5; Gr_θ = 0.78, 1.56, 2.34, 3.12, 3.90

k_∞ = 1.35, 2.35, 3.35, 4.35, 5.35; Gr_C = 1, 3, 5, 7, 9; ϕ = 0.1, 0.2, 0.3, 0.4, 0.5;

K = 0.3, 0.6, 0.9, 1.2, 1.5; ω = 0.2, 0.4, 0.6, 0.8, 1.0; N = 0.5, 1.0, 1.5, 2.0, 2.5;

Pr = 0.71, 1.71, 2.71, 3.71, 4.71; Sc = 0.6, 0.8, 1.0, 1.2, 1.4; t = 0.5; Q = 1

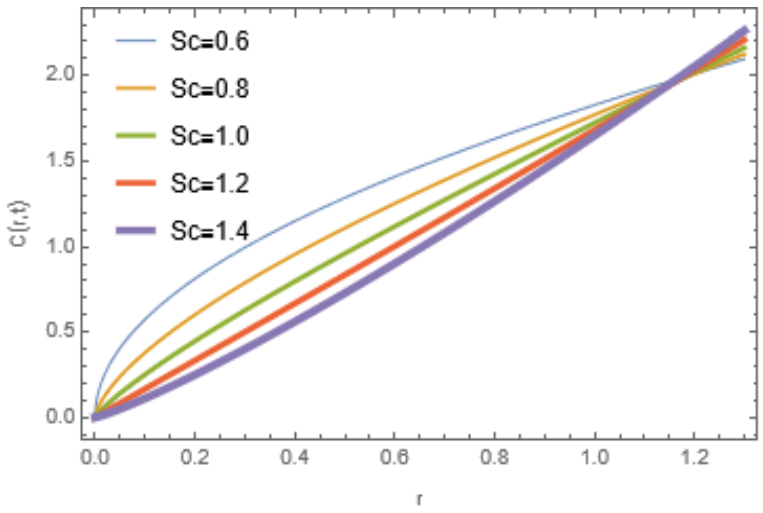

Figure 1: Concentration Profile C against boundary layer r for varying Schmidt number, Sc.

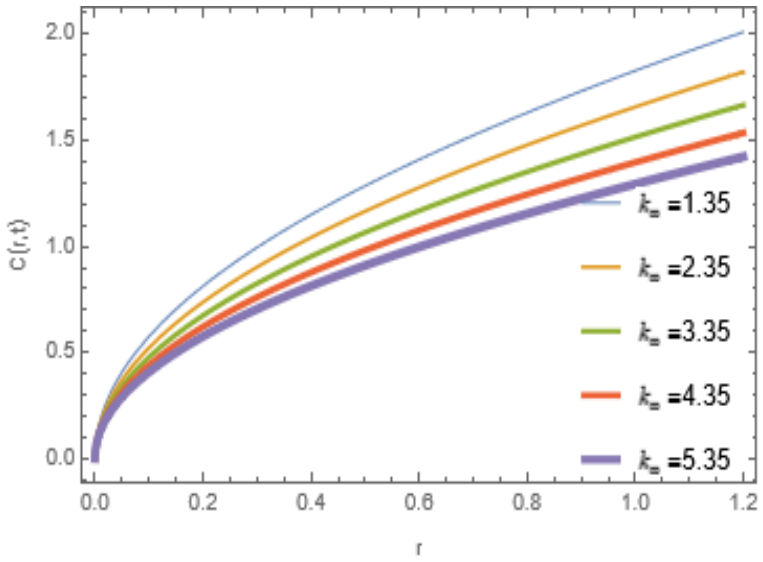

Figure 2: Concentration Profile C against boundary layer r for varying chemical reaction, k_∞.

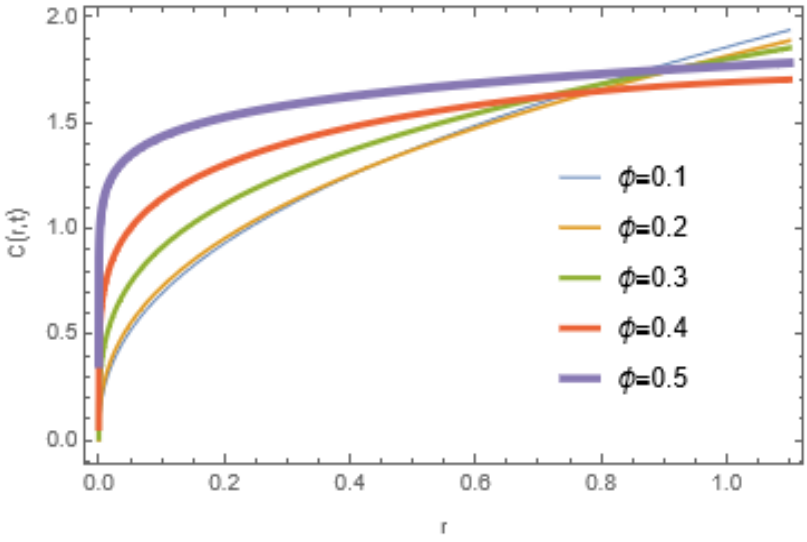

Figure 3: Concentration Profile C against boundary layer r for varying volume fraction, ϕ.

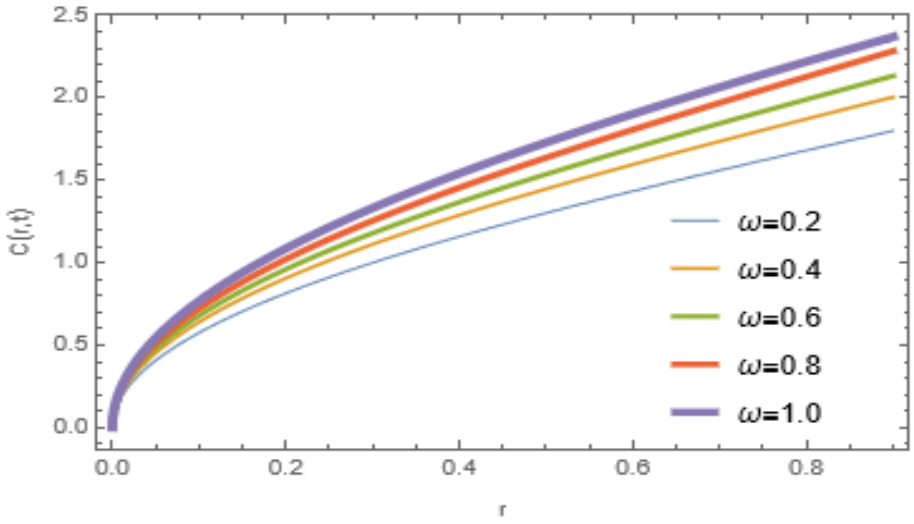

Figure 4: Concentration Profile C against boundary layer r for varying free stream frequency, ω.

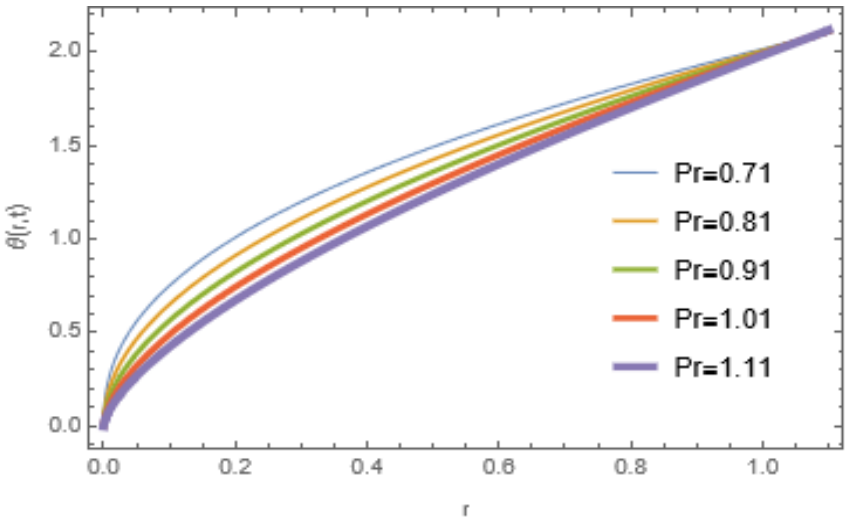

Figure 5: Temperature Profile θ against boundary layer r for varying Prandtl number, Pr.

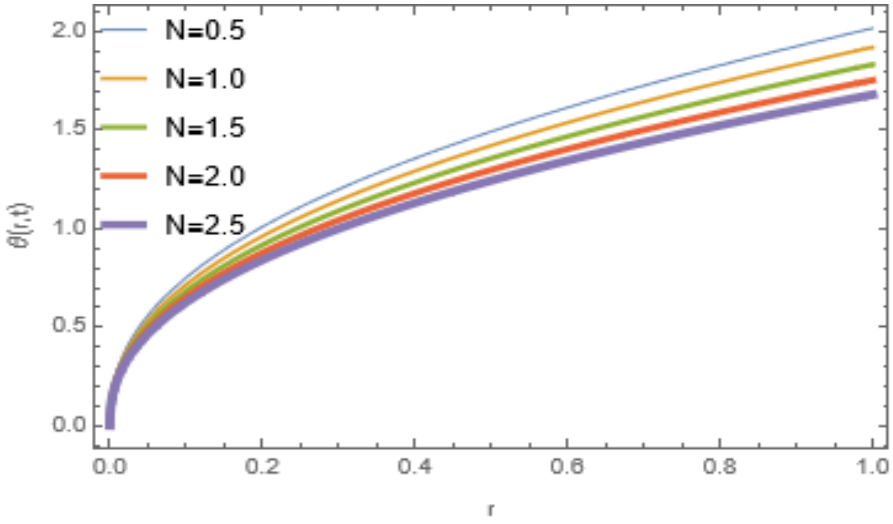

Figure 6: Temperature Profile θ against boundary layer r for varying radiation term, N.

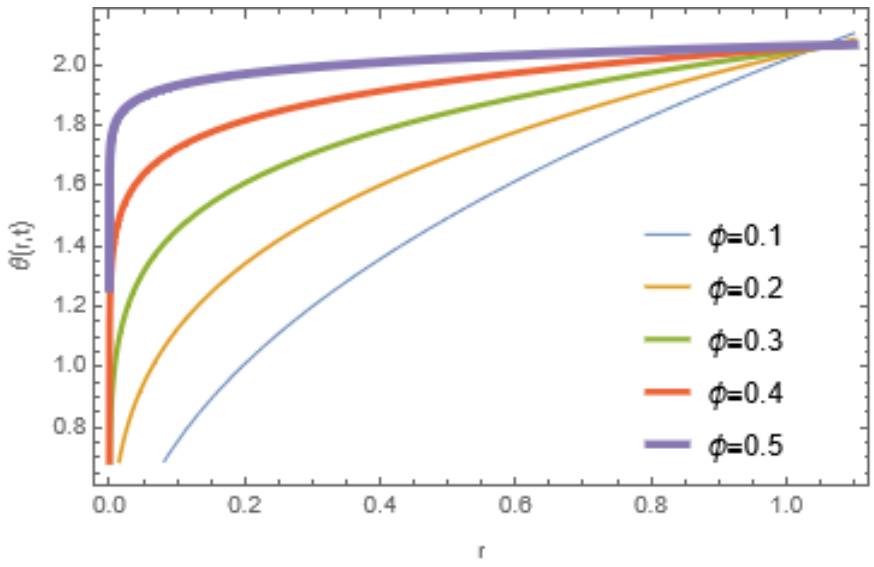

Figure 7: Temperature Profile θ against boundary layer r for varying volume fraction, ϕ.

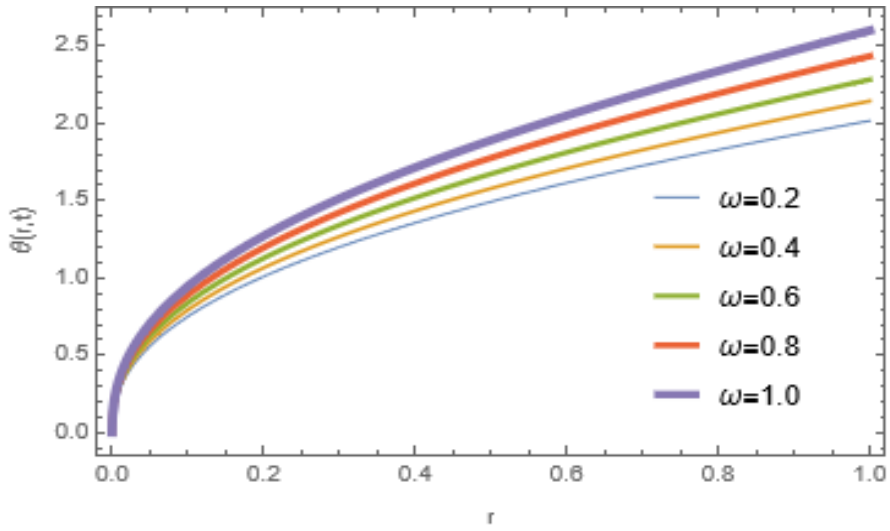

Figure 8: Temperature Profile θ against boundary layer r for varying free stream frequency, ω.

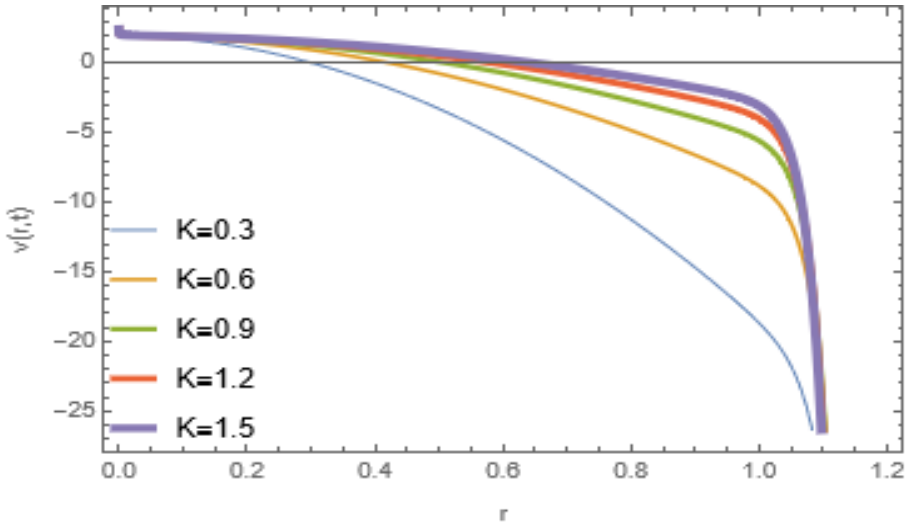

Figure 9: Velocity Profile v against boundary layer r for varying, porosity parameter, K.

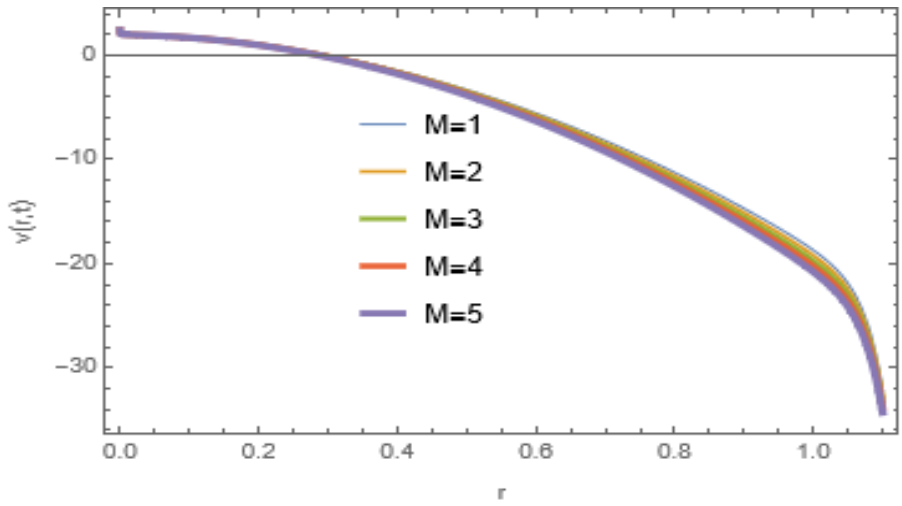

Figure 10: Velocity Profile v against boundary layer r for varying, Magnetic field parameter, M.

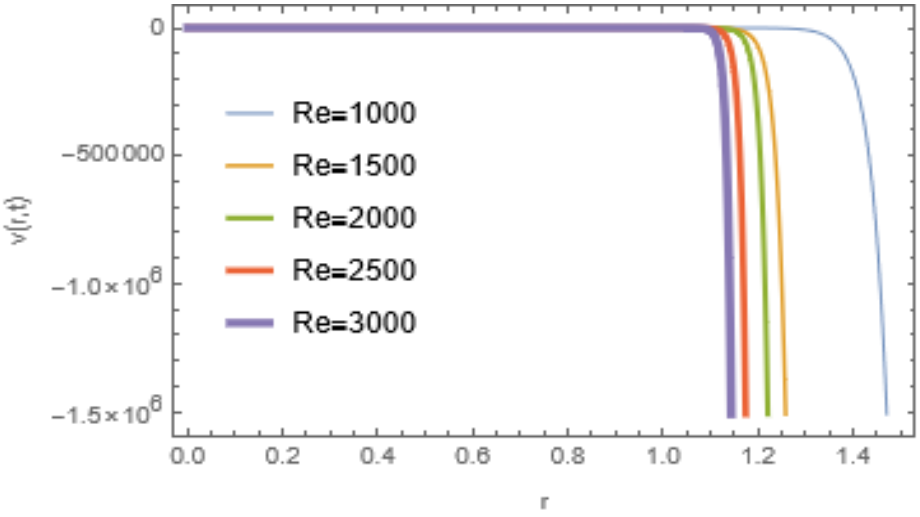

Figure 11: Velocity Profile v against boundary layer r for varying, Reynolds number, Re.

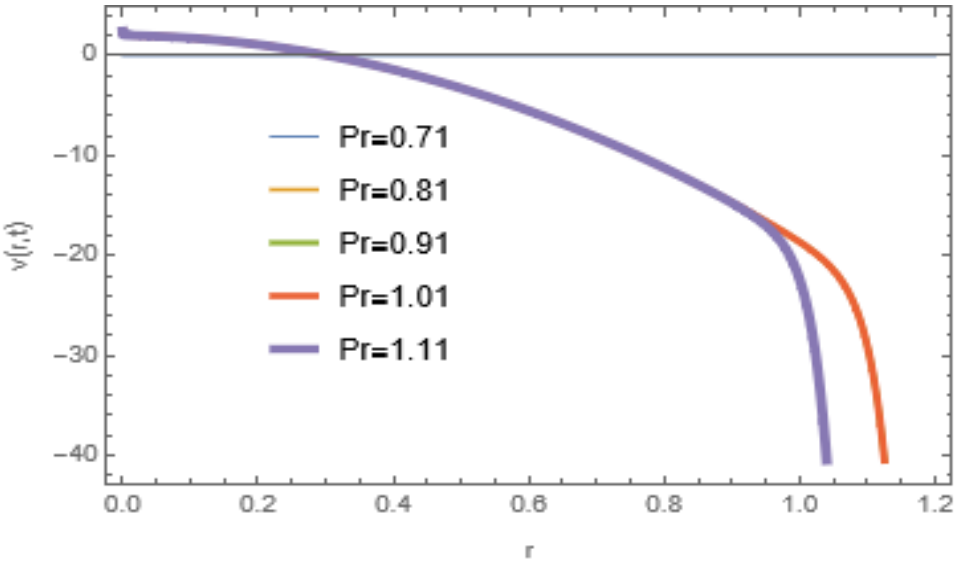

Figure 12: Velocity Profile v against boundary layer r for varying, Prandtl number, Pr.

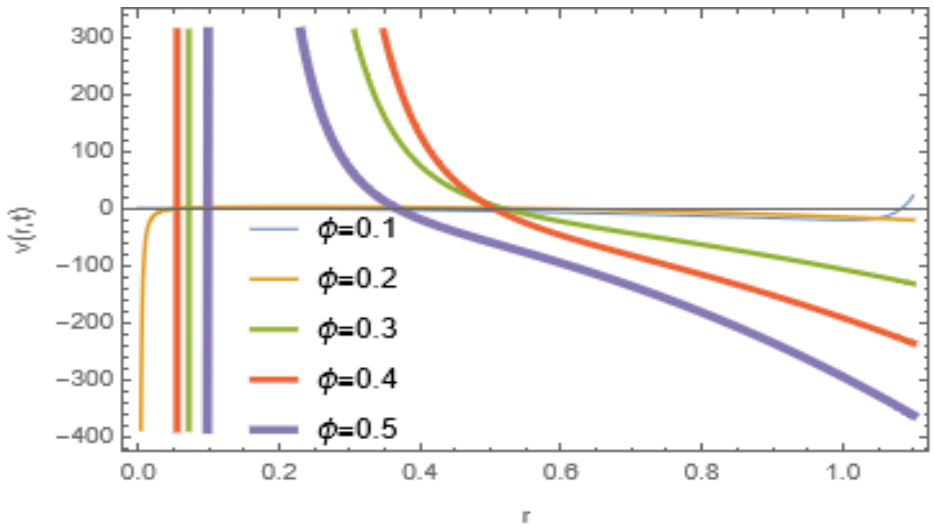

Figure 13: Velocity Profile v against boundary layer r for varying volume fraction, ϕ.

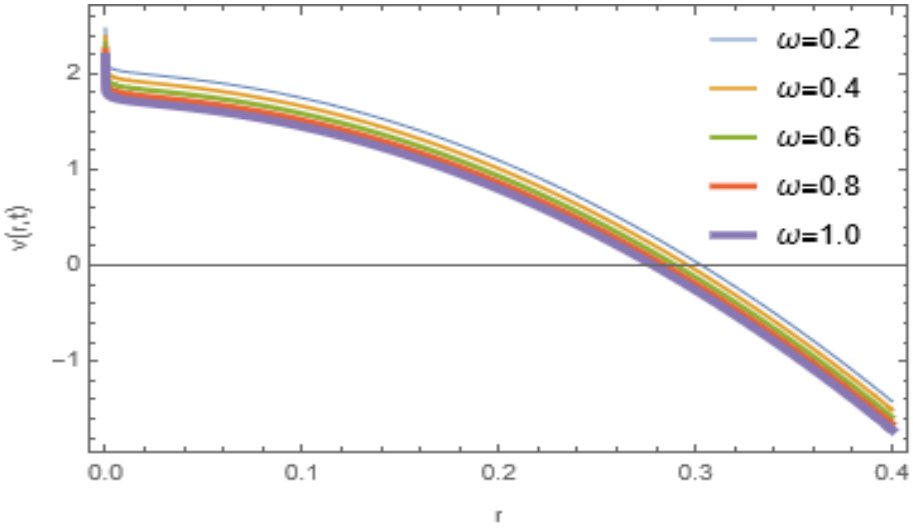

Figure 14: Velocity Profile v against boundary layer r for varying free stream frequency, ω.

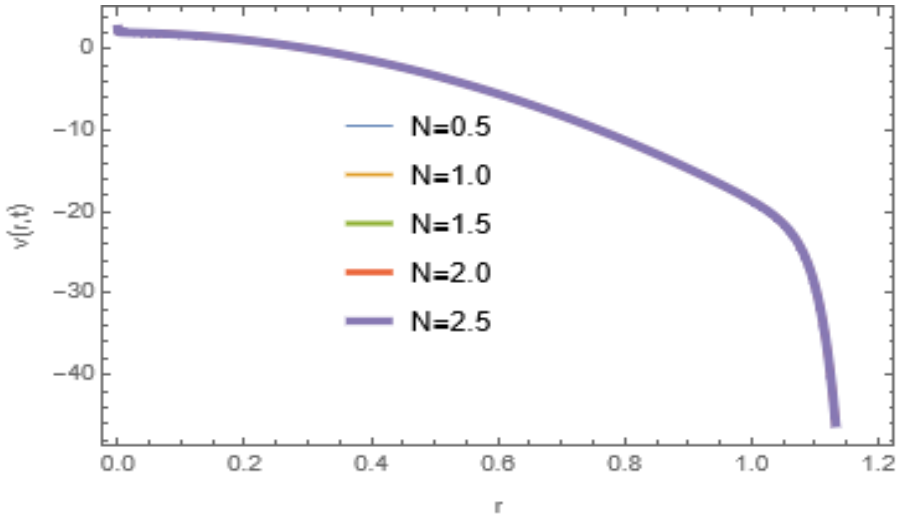

Figure 15: Velocity Profile v against boundary layer r for varying radiation term, N.

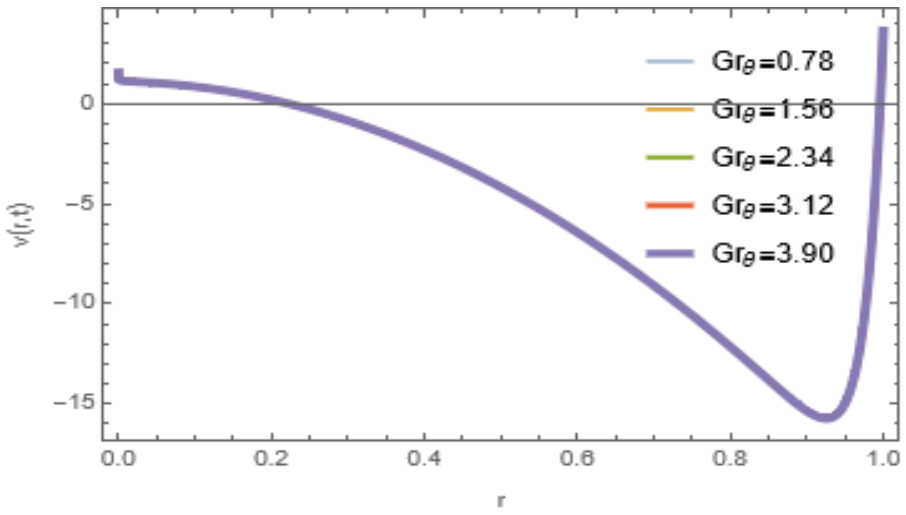

Figure 16: Velocity Profile v against boundary layer r for varying Grashof number, Gr_θ.

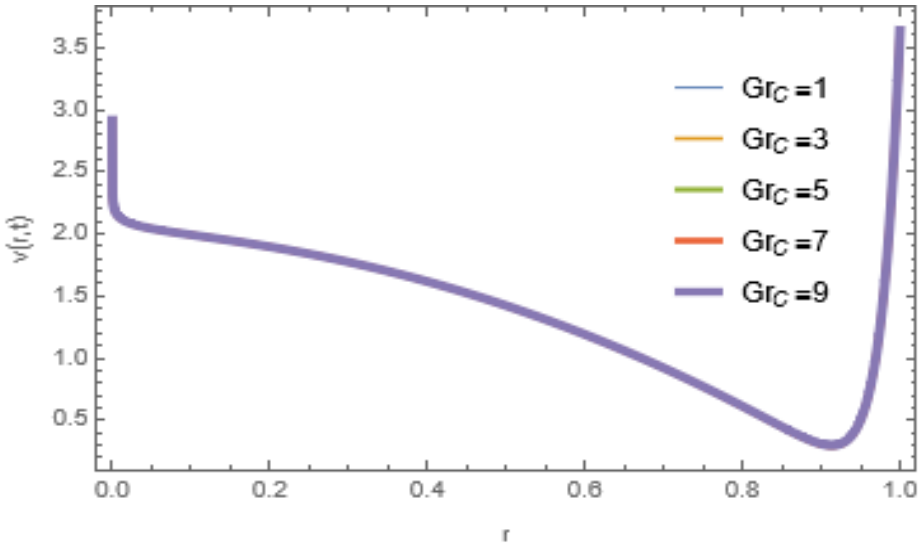

Figure 17: Velocity Profile v against boundary layer r for varying modified Grashof number, Gr_C.

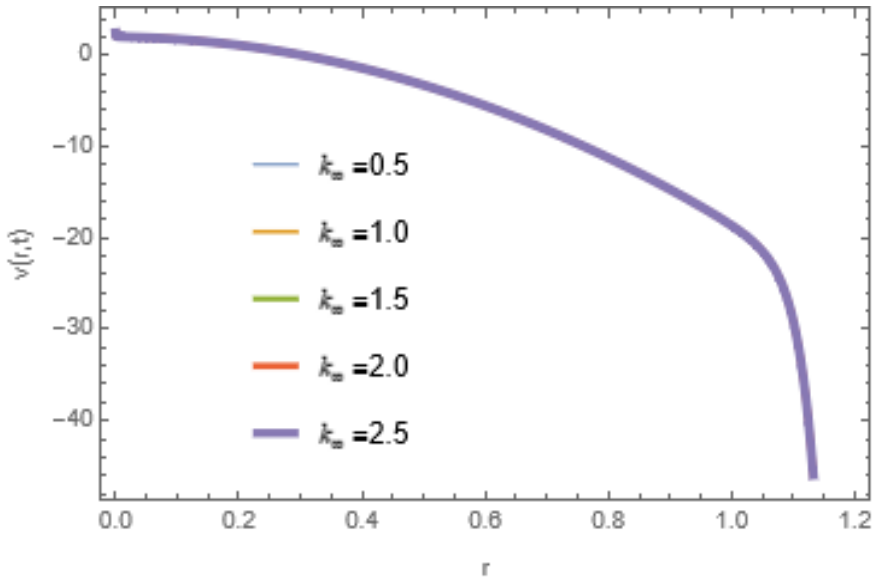

Figure 18: Velocity Profile v against boundary layer r for varying chemical reaction, k_∞.

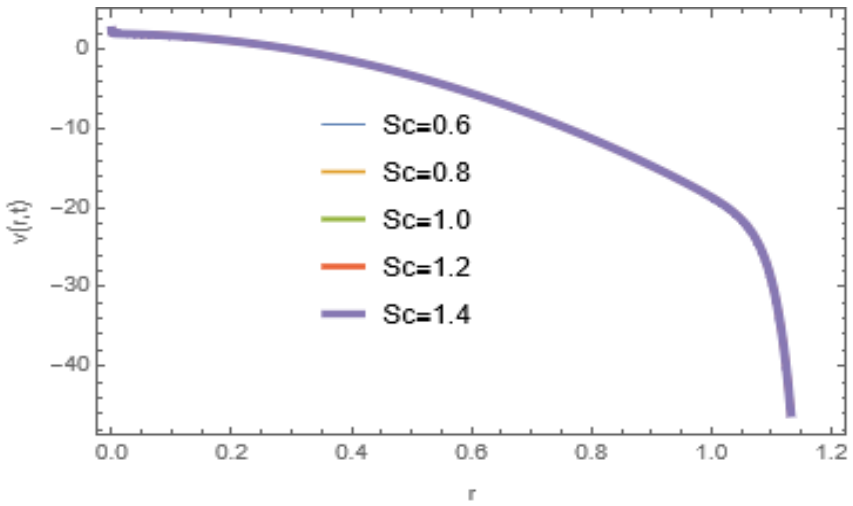

Figure 19: Velocity Profile v against boundary layer r for varying Schmidt number, Sc.

4. DISCUSSION

The Schmidt parameter impact on the concentration is graphically displayed on Figure 1. It was observed that as the Schmidt number is improved upon, there was a decline in the profile of the tin oxide nanofluid concentration, which indicated that the Schmidt parameter decreased the tin oxide nanofluid concentration and it converged at a point. This observation was consistent with the work of Babu et al. (2011).

Figure 2, is the effects of chemical reactions on the tin oxide nanofluid concentration profile. As the chemical reaction progressed, it was observed that the tin oxide nanofluid of concentration profile decreased. The observation was consistent with the work of Babu et al. (2011).

The nanoparticle volume fraction is one of the most significant aspects to consider when describing a nanofluid, and almost every nanofluid parameter is influenced by it. As shown in Figure 3, the tin-oxide nanofluid concentration profile increased as the volume fraction was increasing, and converged at a point. The findings of Ngiangia et al. (2021) are compatible with this observation.

Figure 4, shows that the concentration profile of the tin oxide nanofluid increased as the free stream frequency was increased. The work was consistent with the work of Ngiangia et al. (2021).

Figure 5 dwells on the Prandtl number impact on the profile of the temperature of the tin-oxide nanofluid. It was observed that an increase in the Prandtl number resulted in a corresponding decrease in the temperature profile of the tin oxide nanofluid and later converged. This observation was consistent with the findings of Makinde and Mukutu (2014) and Karthikeyan et al. (2013). The Prandtl number stands for the ratio of thermal diffusivity to momentum diffusivity.

Figure 6 shows that as radiation was increased, the tin oxide nanofluid's temperature decreased. The passive or energetic emission of waves or particles over space is known as radiation. As a result, we can state that increasing the intensity of heat energy in motion lowers the temperature of the tinoxide nanofluid in the scenario from which it originates. The findings are consistent with those of Ngiangia et al. (2021). As a result, it is critical to emphasize that the tin oxide nanofluid should be insulated from much less radiation to achieve faster cooling.

Figure 7, shows that the temperature profile of the tin oxide nanofluid increased as a result of increase in the volume fraction and it converged at a point. The observation was the same as the findings of Ngiangia and Akaezue (2019).

Figure 8, shows that the temperature profile of the tin-oxide nanofluid was increased as the free stream frequency increased.

Figure 9, shows that as the porosity parameter is increased, the velocity profile of the tinoxide nanofluid was improved. This result was consistent with the findings of Aaiza et al. (2015).

Figure 10, reveals that when the velocity profile of the tin oxide nanofluid was diminished, the magnetic field strength within the region of the nanofluid increased. The study of the effect of magnetic field was also reported by Karthikeyan et al. (2013), Ngiangia and Orukari (2021), and Aaiza et al. (2015). A clear indication that the magnetic field term was opposed to the free flow of the tin oxide nanofluid.

Figure 11, results in a decreased in the velocity profile of the tin oxide nanofluid, and this observation was at variance with the results of the increase in the Reynolds number of base fluids. This observation is consistent with the findings of Ngiangia and Akaezue (2019), Masour et al. (2007), and Polidori et al. (2007). The tin oxide nanofluid is a laminar flow.

Figure 12 dwells on the Prandtl number impact on the profile of the velocity of the tin oxide nanofluid. It was noticed that an increase in the Prandtl number results in a corresponding decrease in the temperature profile of the tin oxide nanofluid. This observation was consistent with the findings of Karthikeyan et al. (2013); Makinde and Mukutu (2014).

Figure 13, reveals that the velocity profile of the tin oxide nanofluid increased as a result of increase the volume fraction. The observation was the same as the findings of Ngiangia and Akaezue (2019).

Figure 14, results in a decrease in the velocity profile of the tin-oxide nanofluid as the free stream frequency was increased.

Radiation impact on the velocity profile is depicted in Figure 15 reveals that an increase in radiation reduced the velocity profile of the tin oxide nanofluid.

The impact of the Grashof number on the profile of the velocity is displayed in Figure 16, which reveals that an increase in the Grashof number reduced the velocity profile of the tin oxide nanofluid. An increase in the thermal Grashof number means cooling the cylindrical plates.

The Modified Grashof number impact on the profile of the velocity is displayed in Figure 17. It reveals that an increase in the Grashof number reduces the velocity profile of the tin oxide nanofluid. An increase in the thermal Grashof number means lowering the concentration of the nanofluid around the plates. The modified Grashof number can be explained as a buoyancy force acting on a fluid due to a concentration difference.

The chemical reaction impact on the profile of the velocity is depicted in Figure 18. It was observed that the profile of the velocity tin oxide nanofluid reduced as the chemical reaction increased.

The Schmidt parameter impact on the velocity is illustrated in Figure 19. It was noticed that as the Schmidt number was improved upon, there was a decline in the profile of the velocity, which indicated that the Schmidt parameter decreased the velocity profile of the tin oxide nanofluid.

5. CONCLUSION

Accurately, a study on a model of MHD convective tin-oxide(TiO_2) nanofluid flow over a cylindrical porous plate is made with the behaviour of the various material parameters such as the magnetic field term M, the Prandtl number Pr, the radiation parameter N, the chemical reaction K_∞, the porosity parameter K, the Schmidt number Sh, the Reynolds number Re, the modified Grashof number Gr_C, the Grashof number Gr_θ, the tin-oxide nanoparticles volume fraction, and the free stream frequency been examined and findings shows that the chemical reaction was increased, the nanofluid concentration profile and the velocity profile were concomitantly reduced. When the radiation parameter was raised, the temperature profile dropped, resulting in a quick cooling effect on the nanofluid. The Prandtl number experienced a similar effect, with a decrease in the velocity profile. This meant that the radiation parameter should be increased to have a cooling effect at the nanofluid's temperature. The velocity profile was enhanced with an increase in the porosity parameter. This was, as a result, responsible for the observed increase in the size of the pore spaces of the porous medium. Generally, it was observed that the tin oxide nanofluid concentration profile, temperature profile, and velocity profile all improved as the nanofluid volume fraction increased. One of the most essential parameters in the description of nanofluids has been discovered to be the nanoparticle volume fraction. It was recommended that a further study on a 3D cartesian coordinate system of the nanofluid should be considered.

REFERENCES

[1] Choi, U.S. (1995). Enhancing thermal conductivity of fluids with nanoparticles. *Development and Applications of Non-Newtonian Flows*. Eds. D. A. 99-105.

[2] Li, B.C. (1998). Nanotechnology in China. *Journal of Aerosol Science*, *29*(5/6), 751-755.

[3] Feng, X., Ma, H., & Huang, S. (2006). Aqueous-organic phase-transfer of highly stable gold, silver, and platinum nanoparticles and new route for fabrication of gold nanofilms at the oil/water interface and on solid supports. *Journal of Physical Chemistry B. 110*(25), 12311-12317.

[4] Kulkarni, D, P.Vajjha, R. S., Das, D.K., & Oliva, D. (2008). "Application of Aluminum Oxide nanofluids in Diesel Electric Generator as Jacket Water Coolant. *Journal of Applied Thermal Engineering*, *28*(14–15), 174–178.

[5] Khan, W.A., Ali, M., Shalizad, M., Sultan, F., Irfan, M., & Asghar, Z. (2020). A note on activation energy and magnetic dipole aspects for cross nanofluid subjected to a cylindrical surface. *Applied Nanoscience*, *10*, 3235-3244.

[6] Mukherjee S., & Paria S. (2013). Preparation and Stability of Nanofluids-A Review. *IOSR Journal of Mechanical and Civil Engineering*, *9*(2), 63-69.

[7] Maleki, H., Alsarraf, J., Moghamzadeh, A., Hajabdollah, A., & Sufaei, M.R. (2019). Heat transfer and nanofluid flow over a porous plate with radiation and slip boundary conditions. *Journal of Central South University*, *26*, 1099-1115.

[8] Xuan, Y., & Li, Q. (2003). Investigation on convective heat transfer and flow features of Nanofluids. *Asian Journal of Heat Transfer*, *125*, 151–155.

[9] Jang, S. P., & Choi, S. U. S. (2004). Role of Brownian motion in the enhanced thermal conductivity of nanofluids. *Journal of Applied Physics Letters*, *84*, 4316– 4318.

[10] Lee, S., Choi, S.U.S., Li, S. J.A., & Eastman, J.A. (1999). Measuring thermal conductivity of fluids containing oxide nanoparticles. *Transfer ASME Journal of Heat Transfer*, *121*, 280- 289.

[11] Mokaddes, M., Ali, M.A., & Ahmed, S.S. (2019). Oriented magnetic field effect on mixed convective flow of nanofluid in a grooved channel with internal rotating cylindrical heat source. *International Journal of Mechanical Science*, *151*, 385-409.

[12] Touloukian, Y.S., Powell, R.W., Ho, C.Y., & Kiemens, P.G. (1970). *Thermophysical properties of matter*. Plenum Press.

[13] Yu, W., Xie, H., Chen, L., & Li, L. (2010). Enhancement of thermal conductivity of kerosene-based Fe_3O_4 nanofluids prepared via phase- transfer method. *Colloids and Surfaces A*, *355*(1-3), 109-113.

[14] Hwarig Y., Lee J.K., & Lee C.H. (2007). Stability and thermal conductivity characteristics of nanofluids, *Thermochimica Acta*, *455*(1-2), 70-74.

[15] Zhu H.T., Zhang C.Y., Tang Y.M., & Wang J.X. (2007). Novel synthesis and thermal conductivity of CuO nanofluid. *Journal of Physical Chemistry C.*, *111*(4), 1646-1650.

[16] Li, X., Zhu, D., & Wang, X. (2007). Evaluation on dispersion behavior of the aqueous copper nanosuspensions II, *Journal of Colloid and Interface Science*, *31*(2):456-463.

[17] Hussain, S., Muhammad, S., Au, G., & Naeem, M. (2018). A bioconvection model for squeezing flow between parallel plates containing gyrotactic microorganisms with impact of thermal radiation and heat generation/absorption. *Journal of Advances in Mathematics and Computer Science*. *27*(4), 1-22.

[18] Chamkha, A.J. (2011). Heat and mass from MHD flow over a moving permeable cylinder with heat generation or absorption and chemical reaction. *International scientific publication and Consulting Services*, 1-20. Doi:10.5899/ 2011/can-00109.

[19] Adeniyan, A. (2015). MHD Mixed Convection of a viscous dissipating and chemical reacting stagnation – point flow near a vertical permeable plate in a porous medium with thermal radiation and heat source/sink. *Asian Journal of Mathematics and Applications*, 1-23.

[20] Rawat, S., Kapoor, S., & Bhargava, R. (2016). MHD flow heat and mass transfer of micropolar fluid over a nonlinear stretching sheet with variable micro inertia density, heat flux and chemical reaction in a non-darcy porous medium. *Journal of Applied Fluid Mechanics*, *9*(2), 321-331.

[21] Gupta, A., & Kumar, R. (2007). Role of Brownian motion on the thermal conductivity enhancement of nanofluids. *Applied Physics Letters*, *91*(22), 223102.

[22] Cheng, H., Ding, Y., & Tan, C., (2007). Rheological behavior of nanofluids. *New Journal of Physics*, *9*(10), 269.

[23] Das, S. K., Putra, N., & Roetzel, W. (2003). Pool boiling characteristics of nano-fluids. *International Journal of Heat and Mass Transfer*, *46*(5), 851–862.

[24] Maiga, S. E. B., Chong T., N., Galanis, N., Roy, G., Mare, T., & Coqueux, M. (2006). Heat transfer enhancement in turbulent tube flow using Al_2O_3 nanoparticle suspension. *International Journal of Numerical Methods for Heat and Fluid Flow*, *16*(3), 275–292.

[25] Mansour, R.B., Galanis, N., & Nguyen, C.T. (2007). Effect of uncertainties in physical properties on forced convection heat transfer with nanofluids. *Applied Thermal Engineering 27*(1), 240-249.

[26] Sheikholeslami, M., Ganji, D.D, Javed, M.Y., & Ellahi, R. (2015). Effect of thermal radiation on magnetohydro dynamics nanofluid flow and heat transfer by means of two-phase mode. *Journal of Magnetism and Magnetic Materials*, *374*, 36-43.

[27] Schnack, D.D. (2009*). Lectures in magnetohydrodynamics*. Springer. DOI: 10.1007/978-3-642-00688-3.

[28] Sheikholeslami, M., Jalili, P. & Ganji, D.D. (2018). Magnetic field effect on nanofluid flow between two circular cylinders using AGM. *Alexander Engineering Journal*, *57*(2), 587-594.

[29] Hayat, T., Imtiaz, M., Alsaedi, A., & Kutbi, M.A (2015). MHD three-dimensional flow of nanofluid with velocity slip and nonlinear thermal radiation. *Journal of Magnetism and Magnetic Materials*, *396*(15); 31-37.

[30] Zeeshan, A., Ellahil, R., Siddigui, A.M., & Rahman, H.U. (2012). An investigation of porosity and magnetohydro dynamic flow of non-Newtonian nanofluid in coaxial cylinders. *International Journal of Physical Sciences 7*, 1353-1361.

[31] Srinivas, S. Vijayalakshmi, A., Reddy, S.A., & Ramamoham, T.R. (206). MHD flow of a nanofluid in an expanding or contraction of porous pipe with chemical reaction and heat source/sink. *Propulsion and Power research*, *5*(2), 134-148.

[32] Aminian, E., Moghadasi, H., & Saffari, H. (2020). Magnetic field effects on forced convection flow of a hybrid nanofluid in a cylinder filled with porous media; a numerical study. *Journal of Thermal Analysis and Calorimetry*, *141*, 2019-2031.

[33] Ngiangia, A.T., & Akaezue, N.N. (2019). Heat transfer of mixed convection electroconductivity flow of copper nanofluid with different shapes in a porous microchannel provoked by radiation and first order chemical reaction. *Asian Journal of Physical and Chemical Sciences*, *7*(1), 1-14. Doi:10:9734/AJOPACS/2019/46301

[34] Hamilton, R.L., & Crosser, O.K. (1962). Thermal conductivity of heterogeneous two component systems. *Journal of Industrial and Engineering Chemistry Fundamentals. 1*(3), 187-191.

[35] Loganathan, P., Chand, P.N., & Ganesan, P. (2013). Radiation effects on an unsteady natural convection flow of a nanofluids past an infinite vertical plate. *NANO 08:1350001.* doi:10.1142/S179329201350001X.

[36] Asma, K., Khan, I., & Sharidan, S. (2015). Exact solutions for free convection flow of nanofuids with ramped wall temperature. *The European Physical Journal Plus*, *130*, 57-71.

[37] Makinde O.D., & Mhone P.Y. (2005). Heat transfer to MHD oscillatory flow in a channel filled with porous medium. *Romanian Journal of Physics*, *50*, 931-938.

[38] Cogley, A.C., Vincent, W.G., & Giles, S.E. (1968). Differential approximation to radiative heat transfer in a non-grey gas near equilibrium. *The American Institution Aeronautics and Astronautics*. *6*, 551-553.

[39] Timofeeva, E.V., Routbort, J.L., & Singh, D. (2009). Particle shape effects on thermophysical properties of alumina nanofluids. *Journal of Applied Physics*, *106*(1), 014304.

[40] Aaiza, G., Khan, I., & Shafie, S. (2015). Energy transfer in mixed convection MHD flow of nanofluid containing different shapes of nanoparticles in a channel filled with saturated porous medium. *Nanoscale Research Letters*, *10*(1), 1-14.

[41] Ngiangia, A.T., & Orukari, M. A. (2021). Heat transfer coefficient and skin friction determination of thermal radiation effects on MHD convective flow of alumina nanofluid through a non-Darcian porous plate. *International Journal of Scientific & Engineering Research*, *12*(5), 355-378.

[42] Dass, H.K., & Rama, V. (2000). *Mathematics physics*. S. Chand & Company Ltd.

[43] Gupta, B.D. (2005). *Mathematical physics (third revised edition).* Viskas Publishing House PVT LTD.

[44] Raisinghania, M.D. (2011). Advanced differential equations (Fourth Revised Edition). S. Chand and Company LTD.

[45] Babu, M.S, Narayana, P.V.S, Reddy, T.S., & Reddy, D.U (2011). Radiation and chemical reaction effects on an unsteady MHD convection flow past a vertical moving porous plate embedded in a porous medium with viscous dissipation. *Advances in Applied Science Research*, *2*(5), 226-239.

[46] Ngiangia, A.T., Orukari, M. , Amadi, O., & Nwabuzor, P. (2021). Onset of transition to non-Newtonian MHD chemically reacting couette copper nanofluid flow in a radiative porous medium. *International Journal of Mathematics Trends and Technology*, *67*(5); 126-149. Doi:10.4445/22315373/IJMTT-V6715p515

[47] Makinde, O.D., & Mukutu, W.N. (2014). Hydromagnetic thermal boundary layer of nanofluids over a convectively heated flat plate with viscous dissipation and ohmic heating. *Science Bullettin Series A, 76*(2), 181-192.

[48] Karthikeyan, S., Bhuvaneswari, M., Rajan, S., & Sivasankaran, S. (2013). Thermal radiation effects on MHD convective flow over a plate in a porous medium by perturbation technique. *Applied Mathematics and Computational Intelligence 2*(1); 75-83.

[49] Mansour, R.B., Galanis, N., & Nguyen, C.T. (2007). Effect of uncertainties in physical properties on forced convection heat transfer with nanofluids. *Applied Thermal Engineering 27*(1), 240-249.

[50] Polidori, G., Fohanno, S., & Nguyen, C.T. (2007). A note on heat transfer modeling of Newtonian nanofluids in laminar free convection. *International Journal of Thermal Sciences 46*(8), 739-744.